ISBN: 978-981-94-1156-6
2024 the 14th International Workshop on Computer Science and Engineering (WCSE 2024)
doi: 10.18178/wcse.2024.06.034

PFM-based Soft Switching Implementation with Reverse Conduction Control

Zhihao Kang, Cheng Lei and Jian Zhang+

School of Automation, Wuhan University of Technology, Wuhan, China

Abstract. With the rapid development of mobile communication, satellite communication and radar field, resonant power converter is widely used, and the demand of all kinds of equipment is increasing, and the requirement of its ability to cope with all kinds of conditions in different application scenarios is also increasing, and the development trend of power converter is becoming the trend of ultra-high frequency and flexible application. However, if the input voltage, output load or ambient temperature fluctuates significantly, the resonant network parameters may change, resulting in the soft switching conditions in the converter are no longer satisfied or even invalid; in the traditional PFM control, the converter switches between different operating modes whenever the switch is disconnected, and if there is a large current or voltage, a reverse bias may be generated in the switch, resulting in reverse conduction loss. To solve the problems caused by the above reasons, this paper proposes a BDPFM optimal control method based on PFM, which ensures the effective operation of the soft switch and avoids the reverse conduction of the device. Compared with the traditional control strategy.

Keywords: BDPFM; soft switching; reverse conduction; optimal control Introduction.

1. Introduction

In recent years, some progress has been made in the research of soft switching realization and reverse conduction control based on PFM, but the rectifier stage load and the UHF resonant power converter under PFM control still lead to more problems when the operating conditions change, especially in the UHF operating environment, the reverse conduction loss will be very significant, which makes the amplitude of the currents and voltages in the instant of shutting off and turning on increase.

To optimize the stability of the converter under high-frequency conditions, scholars at home and abroad have studied the modelling and optimization of ultra-high-frequency resonant power converters. Optimization of the circuit structure is proposed in paper [5]: by improving the circuit topology, the losses in the circuit are reduced and the efficiency of the circuit is improved, and three control methods based on space vectors are established; optimization of the control strategy is proposed in paper [8]: advanced control strategies, and adaptive control, fuzzy control, etc. are adopted to improve the dynamic response speed and stability of the converter. The above methods can ensure the realization of soft-switching under different operating conditions under ON/OFF control, but the output ripple is large; soft-switching failure occurs at the optimum point of frequency offset under conventional control.

Based on the above problems, this paper firstly establishes a simplified model of isolated ultra-high frequency resonant power converter based on the resonance fitting method, optimizes the design of the resonant network, adopts the descriptive function to model the rectifier as a variable resistance and inductance, and reduces the order of the resonant network based on the impedance you sum to obtain the simplified circuit model, and then solves the time-domain solution of the circuit under dynamic switching frequency. On this basis, a BDPFM optimal control method is proposed to calculate the critical duty cycle based on the real-time operating frequency to ensure the realization of the power tube ZVS and avoid the reverse conduction of GaN HEMT devices. Combining the above analyses, the BDPFM schematic block diagram can be proposed to achieve ZVS and avoid reverse conduction of power devices. It is shown in Fig1.

+ Corresponding author. Tel.: +86 15697170258.
E-mail address: 1655517759@qq.com.

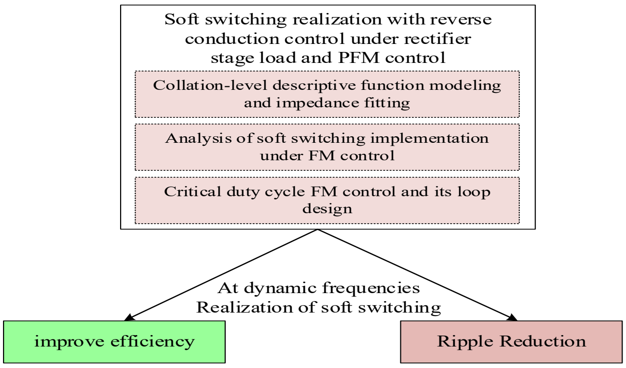

Fig.1: BDPFM controller block diagram

2. Power Topology Model Based on Resonance Fitting

To ensure the ZVS operating state of the power tube and avoid reverse conduction loss, the time domain solution of the circuit at different switching frequencies needs to be solved. However, it is difficult to analyze the circuit directly due to the existence of four states (switching and diode conduction) and multiple resonant elements. To solve the problem of solving the time-domain solution of the circuit at different switching frequencies, this paper establishes a resonance fitting model for the UHF isolated resonant power converter. The model derivation process is shown in Fig 2.

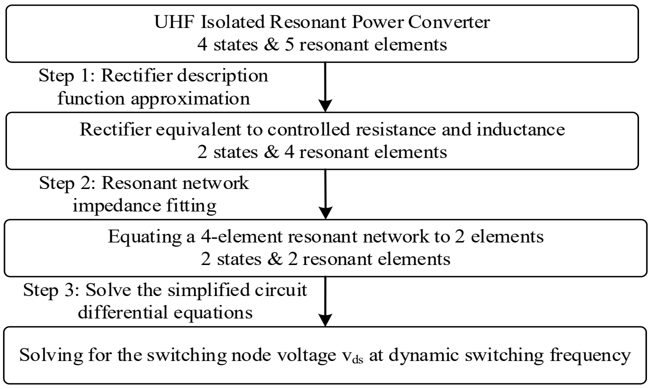

Fig. 2: Resonance fitting model derivation process

2.1. Theoretical Foundations

The input impedance of the rectifier is designed to be purely resistive, which enables the rectifier to maintain a linear relationship between the input voltage and current waveforms at the switching frequency, thus better controlling the stable operation of the rectifier; and reduces the harmonic disturbances, improves the quality of the power supply, and makes the energy transfer more efficient and reduces the energy loss. Therefore, in conventional modelling, the rectifier is usually modelled as a resistor. However, when the frequency control method is used, the input impedance of the rectifier will be shifted with the change of switching frequency, which leads to a large error in the time-domain analysis results.

To solve the above problems, this section adopts the describing function method to model the rectifier as a controlled resistor and inductor, as shown in Fig.3.

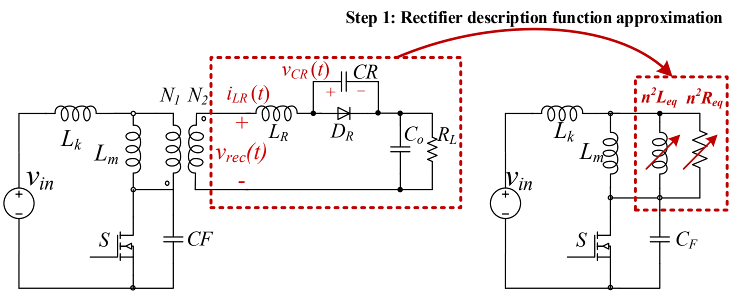

Fig. 3: Modelling rectifiers as controlled inductors and resistors based on descriptive functions

The input voltage of the rectifier can be approximated as:

$$V_{rec}(t) = V_R \sin(\omega_S t + \theta) \tag{1}$$

Where θ is the initial phase of $v_{rec}(t)$ and $v_R(\omega_S)$ denotes the input voltage amplitude of the rectifier, which can be calculated from the base wave amplitude of the output voltage of the inverter. The rectifier has two operating modes: diode conduction mode and diode turn-off mode. The rectifier satisfies the following equation when the diode is turned off during $t \in (0, to_{offrec}]$:

$$\begin{cases} L_R \dfrac{di_{LR}(t)}{dt} + V_{CR}(t) + V_0 = V_r \sin(\omega_S t + \theta) \\ C_R \dfrac{dV_{CR}(t)}{dt} = i_{LR}(t) \end{cases} \tag{2}$$

The above differential equation should satisfy the following two boundary conditions: (1) The diode switches off at moment 0. (2) The diode realizes ZCS. i.e.

According to the above boundary conditions, the analytical solution of the rectifier in the diode-off stage can be obtained. During $t \in (t_{offrec}, T]$ the diode conducts and the rectifier satisfies the following differential equation:

$$\begin{cases} L_R \dfrac{di_{LR}(t)}{dt} + v_D + v_0 = v_R \sin(\omega_S t + \theta) \\ v_{CR}(t) = v_D \end{cases} \tag{3}$$

The analytical expression for the resonant capacitor voltage $v_{CR}(t)$ is given by:

$$v_{CR}(t) = \begin{cases} \dfrac{\left(\begin{array}{l} C_R v_R \omega_s\, cos(\theta)\, cos(\frac{t}{\sqrt{C_R L_R}}) - C_R v_R \omega_s\, cos(\omega_s t + \theta) \\ + \sqrt{\frac{C_R}{L_R}}((v_o + v_D)(1 - C_R L_R {\omega_s}^2) - v_R\, sin(\theta))\, sin(\frac{t}{\sqrt{C_R L_R}}) \end{array} \right)}{(-1 + C_R L_R {\omega_s}^2)} \\ v_D \end{cases} \tag{4}$$

The analytical expression for the resonant inductor current $i_{LR}(t)$ is given by:

$$i_{LR}(t) = \begin{cases} -v_o + (v_o + v_D)\, cos(\frac{t}{\sqrt{C_R L_R}}) + \dfrac{-v_R\, sin(\omega_s t + \theta)}{-1 + C_R L_R {\omega_s}^2} \\ + \dfrac{v_R\, cos(\frac{t}{\sqrt{C_R L_R}})\, sin(\theta) + \sqrt{C_R L_R} v_R \omega_s\, sin(11 \frac{t}{\sqrt{C_R L_R}})\, cos(\theta)}{(-1 + C_R L_R {\omega_s}^2)} \\ i_{LR}(t_{offrec}) - \dfrac{v_o + v_D}{L_R}(t - t_{offrec}) \\ + \dfrac{v_R(cos(\omega_s t_{offrec} + \theta) - cos(\omega_s t + \theta))}{L_R \omega_s} \end{cases} \tag{5}$$

The above analytical solution should satisfy the following two boundary conditions. (1) At the moment $t = t_{offrec}$, the voltage across the resonant capacitor resonates to the forward conduction voltage drop v_D and the diode naturally conducts, i.e., $v_{CR}(t_{offrec}) = v_D$. (2) The inductor current is continuous when the rectifier operates in steady state, i.e., the resonant current at the beginning of the switching cycle should be equal to the resonant current at the end of the switching cycle, i.e., $i_{LR}(0) = i_{LR}(T)$. The unknowns t_offrec and θ in the above analytical expression can be found by substituting the above boundary conditions into Eq. (4) and Eq. (5).

Further, by performing a Fourier analysis of the rectifier input current $i_{LR}(t)$, the describing function of the rectifier can be calculated as follows. The resistive input current and the inductive input current of the rectifier are the projections of $i_{LR}(t)$ on $sin(\omega_S t+\theta)$ and $-cos(\omega_S t+\theta)$, respectively, which are computed as:

$$\begin{cases} i_{LR,res} = \dfrac{2}{T}\displaystyle\int_0^T i_{LR}(t)\sin(\omega_S t+\theta)\,dt \\ i_{LR,ind} = \dfrac{2}{T}\displaystyle\int_0^T -i_{LR}(t)\cos(\omega_S t+\theta)\,dt \end{cases} \tag{6}$$

Where T denotes the switching period of the converter, i_{LRres} is the current generated by the resistive component of the rectifier input characteristic, and i_{LRind} is the current generated by the reactive component of the rectifier input characteristic. According to the magnitude of the resistive and inductive currents obtained from equation (7) that is, the descriptive function of the rectifier can be calculated as:

$$N(\omega_s) = R_{eq}(\omega_s)||j\omega_s L_{eq}(\omega_s) = \frac{j\omega_s L_{eq}(\omega_s)R_{eq}(\omega_s)}{j\omega_s L_{eq}(\omega_s)+R_{eq}(\omega_s)} \tag{7}$$

Where $R_{eq}(\omega_s)$, $L_{eq}(\omega_S)$ are given by equation (8).

$$\begin{cases} R_{eq}(\omega_S) = \dfrac{v_R(\omega_S)}{i_{LR,res}} \\ L_{eq}(\omega_s) = \dfrac{v_R(\omega_S)}{i_{LR,ind}\,\omega_S} \end{cases} \tag{8}$$

Based on the above calculations and considering the turns ratio of the transformer $n = N_1/N_2$, the rectifier can be modelled as a controlled resistance and inductance in parallel. The rectifier is modellaed using a descriptive function to simplify the original 4-state, 5-resonant-element UHF isolated resonant power converter to a 2-state, 4-resonant-element equivalent circuit.

2.2. Impedance Fitting of Resonant Networks

The impedance characteristics of the resonant network at the switching frequency. Fitting the resonant slot impedance characteristics using a simple network can further simplify the calculation. In this section, R_P, L_P are used to approximate the resonant slot impedance $Z_{inv}(j\omega)$ by fitting, to further simplify the equivalent circuit, as shown in Fig. 4.

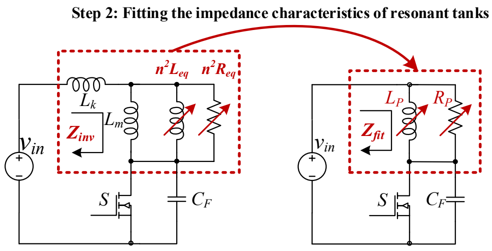

Fig. 4: De-ordering of resonant networks based on impedance fitting

The analytical expressions for R_P and L_P can be foaund as:

$$\begin{cases} L_P = \dfrac{R_S^2}{L_S\omega_S^2} + L_S \\ R_P = R_S + \dfrac{L_S^2\omega_S^2}{R_S} \end{cases} \tag{9}$$

Where the values of L_S and R_S are taken, respectively:

$$\begin{cases} L_S = L_k + \dfrac{n^4 L_{eq} R_{eq} L_m (n^2 L_{eq} R_{eq} + L_m R_{eq})}{(n^3 L_{eq} R_{eq} + n L_m R_{eq})^2 + (\omega_S n L_m L_{eq})^2} \\ R_S = \dfrac{n^4 \omega_S^2 R_{eq} L_{eq}^2 L_m^2}{(n^3 L_{eq} R_{eq} = n L_m R_{eq})^2 + (\omega_S n L_m L_{eq})^2} \end{cases} \tag{10}$$

Then the time domain solution of the converter can be solved based on the simplified circuit model shown in Fig.5 as follows:

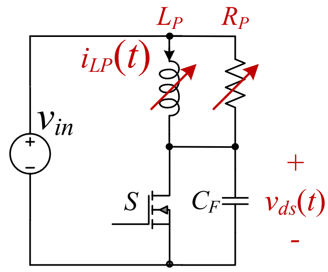

Fig. 5: Simplified Circuit for UHF Isolated Resonant Power Converter

The analytical expression for the resonant current of inductor L_P is:

$$i_{LP}(t) = \begin{cases} \dfrac{\begin{pmatrix} c_2 e^{(-\alpha+\beta)t}(1 - \alpha C_F R_P + \beta C_F R_P) \\ -c_1 e^{(-\alpha-\beta)t}(-1 + \alpha C_F R_P + \beta C_F R_P) \end{pmatrix}}{R_P} & 0 < t \le t_{offinv} \\ i_{LP}(t_{offinv}) + \dfrac{v_{in}}{L_P}(t - t_{offinv}) & t_{offinv} < t \le T \end{cases} \tag{11}$$

The analytical expression for the switching node voltage is:

$$v_{ds}(t) = \begin{cases} v_{in} + c_1 e^{(-\alpha-\beta)t} + c_2 e^{(-\alpha+\beta)t}, & 0 < t \le t_{offinv} \\ 0 \qquad\qquad\qquad\qquad\qquad\quad , & t_{offinv} < t \le T \end{cases} \tag{12}$$

The results of the switching node voltage waveform calculations under different switching frequencies are given in Fig.6, and the circuit parameters used in the calculations are consistent with the experiments.

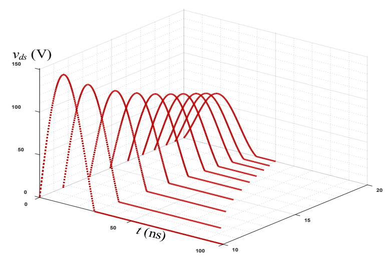

Fig. 6: Switching node voltage waveforms at different switching frequencies

According to the above results, the critical duty cycle for realizing soft switching under different switching frequencies can be calculated, which provides a theoretical basis for the proposed control strategy.

3. Soft Switching Implementation Analysis and BDPFM Control Strategy

In order to improve the efficiency of ultra-high frequency isolated resonant power converter, the power tube turn-on timing is very critical. If the duty cycle of the gate drive signal is large, it will lead to soft-switching failure. For this reason, this section proposes the BDPFM control strategy, which selects the critical duty cycle according to the real-time operating conditions of the converter, to realize the soft-switching of the power tubes.

Based on the previous section, the critical duty cycle for soft-switching at dynamic switching frequency can be calculated, and the small-signal model of the power converter under FM control can be established according to the BDPFM control strategy, which gives the basis for the parameter design of the control loop. To broaden the load range of the converter, it is switched to ON/OFF control at light load. The control block diagram is shown in Fig 7.

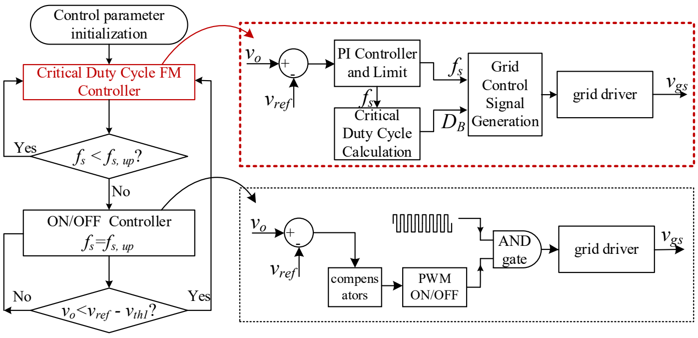

Fig. 7: The complete block diagram of the control method proposed in this paper

The initial operating state of the converter is BDPFM control, and if the switching frequency reaches the upper limit $f_{s.up}$ it indicates that it enters the light load state, and the control mode switches to ON/OFF control. In this state, when the output voltage is lower than the set threshold, i.e., $V_O < V_{ref} - V_{th1}$, it indicates that the converter under ON/OFF control is not able to provide a large enough output power, and the control mode switches back to BDPFM control.

3.1. Theoretical Calculation

Under frequency control, the critical duty cycle is transformed with frequency adjustment. According to the zero-crossing point of the switching node voltage at different switching frequencies, the critical duty cycle to achieve soft switching can be found.

Turning on the power tube immediately after the switching node voltage resonates to 0 can ensure soft switching while avoiding reverse conduction loss. The resonance crossing point of $v_{ds}(t)$ can be found as t_{offinv} by making the switching node voltage $v_{ds}(t) = 0$. Turning on the power tube at the moment of t_{offinv} and switching off the power tube after one cycle T can realise the soft switching of the power tube and avoid the reverse conduction loss. As shown in Fig.8.

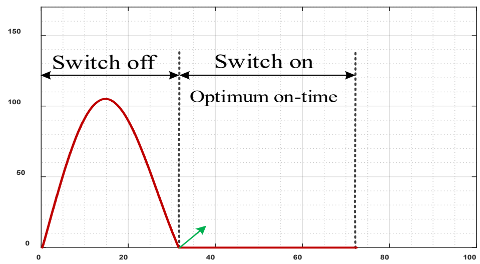

Fig. 8: Switching Node Voltage Waveforms with Critical Duty Cycle

The variation of t_{offinv} and D_B with switching frequency f_S is shown in Fig.9.

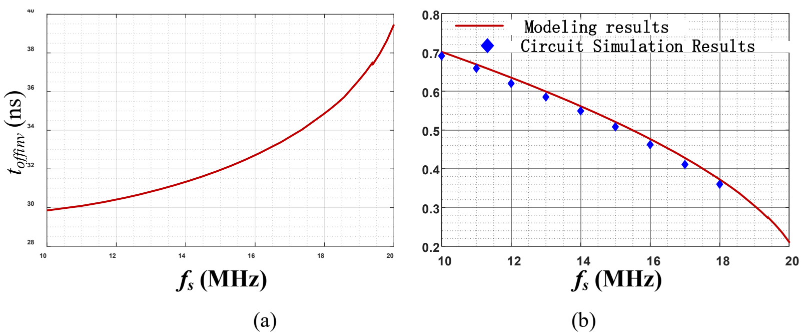

Fig. 9: The variation with switching frequency of t_{offinv} and D_B: (a) t_{offinv}; (b) D_B

The parameters used in the calculations are consistent with those in the experiments. It can be seen that the critical duty cycle decreases as the switching frequency increases. Based on this result, the critical duty cycle can be calculated based on the real-time switching frequency of the converter to achieve the ZVS of the power tube while avoiding the reverse conduction of the GaN HEMT.

The trend of the output power P0 of the converter with operating frequency is shown in Fig.10.

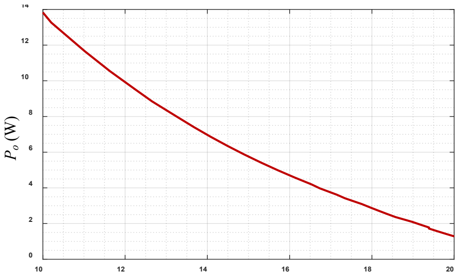

Fig. 10: Variation of output power with operating frequency

It can be obtained that the output power of the converter monotonically decreases with the increase of the switching frequency over the operating frequency range of the converter and there is a one-to-one mapping functional relationship.

Therefore, it is possible to control the switching frequency of the converter through the Vanquish loop to achieve output voltage regulation control. The above analysis provides a theoretical basis for BDPFM control.

3.2. Control Implementation and Loop Design

Based on the calculation results in the previous section, the BDPFM controller schematic block diagram can be proposed.

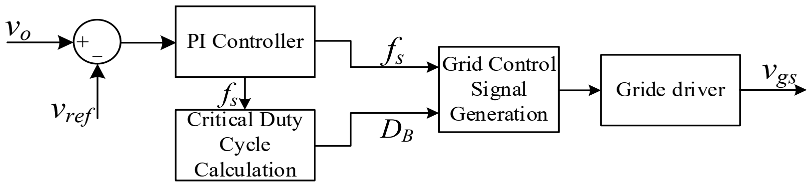

Fig. 11: BDPFM Controller Block Diagram

The PI controller is a proportional-integration controller (PI controller) that adjusts the converter's operating frequency, f_S, according to the error between the output voltage and the reference voltage; the critical duty cycle calculation module can calculate the corresponding critical duty cycle, D_B, according to the real-time common-coupled operating frequency, f_S. f_S and D_B together determine the gate control signal of the power tube, and the control signal is connected to the gate of the power tube after the gate driver increases the driving capability. f_S and D_B together determine the gate control signal of the power tube, and the control signal is connected to the gate of the power tube after the gate driver increases the driving capability.

For ultra-high frequency resonant power converters, the resonant capacitance and resonant inductance are usually in the order of $100pF$ and $100nH$, while the output capacitance is usually in the order of $10\mu F$. Thus, compared to the output capacitance, the effect of the resonant inductance and the resonant capacitance on the dynamic performance of the converter can be neglected, and the main poles of the system are determined by the output capacitance and the load resistance. Further, the main power topology under FM control can be equated to a controlled current source. In summary, a small-signal model of the ultra-high isolated resonant power converter under FM control can be established as shown in Fig.12.

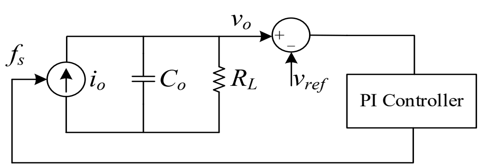

Fig.12: Small-signal modeling of an ultrahigh-frequency isolated resonant power converter under frequency modulation control

Accordingly, the open-loop transfer function $G_{vf}(s)$, $G_{if}(s)$ can be picked f_s to i_O DC gain $G_{if}(0)$ approximation, and the dynamic response speed of the converter is mainly determined by the output poles, so the system transfer function can be approximated as:

$$G_{vf}(s) = G_{if}(0)\frac{R_L}{1+sR_LC_0} \tag{13}$$

Where $G_{if}(0)$ is calculated as:

$$G_{vf}(0) = \frac{\partial i_0}{\partial f_S} = \frac{\partial\sqrt{P_0/R_L}}{\partial f_S} = \frac{1}{2}\sqrt{\frac{1}{R_LP_0}\frac{\partial P_0}{\partial f_S}} = \frac{1}{2v_0}\frac{\partial P_0}{\partial f_S} \tag{14}$$

To ensure the stability of the system in the full range, the maximum value of the slope of the curve is used as the value of $\partial P_o/\partial f_S$. According to the MATLAB calculation, the maximum value of the slope of the curve in Fig.11 is $max(\partial P_o/\partial f_S)$ =-2.9 W/MHz.Substituting this calculation and the experimental parameter $v_O = 5\,V$ into Eq. (14) yields $G_{if}(0) = -0.29A/MHz$.

Under PI control, the loop gain of the system is:

$$\Phi_{LP}(s) = G_{vf}(s)G_{PI}(s) = \frac{G_{if}(0)R_L}{1+sR_LC_0}\frac{sk_p+k_i}{s} = \frac{G_{if}(0)k_p}{sC_0}\frac{s+k_i/k_p}{s+1/(R_LC_0)} \tag{15}$$

Where k_p, k_i are the proportional and integral coefficients of the PI controller respectively. According to the form of Eq. (16), the main pole of the system can be offset by setting the zero position of the PI controller; the desired loop bandwidth ω_n can be obtained by setting the parameter sizes of the PI controller. therefore, the control parametersk_p, k_i of the PI controller should be satisfied:

$$\begin{cases} k_p = \dfrac{\omega_n C_0}{G_{if}(0)} \\ k_i = \dfrac{\omega_n}{G_{if}(0)R_L} \end{cases} \tag{16}$$

4. Experimental Validation of BDPFM Control Strategy

To verify the effectiveness of the BDPFM control strategy proposed in this paper, a UHF isolated resonant power converter model is constructed on a simulation platform.

4.1. Homeostasis Experiment

In this paper, the operating frequency of the converter is 12.08 MHz at 100% load, and the critical duty cycle is 0.63. Due to the critical duty cycle, the power tubes are turned on immediately after v_{ds} resonates to 0, which ensures the realisation of the ZVS of the power tubes and avoids their reverse conduction. At 40% load, the operating frequency of the converter is increased to 16.7 MHz, and at the same time, the duty cycle is adjusted to 0.42. Similarly, the power tubes are turned on as soon as v_{ds} resonates to zero. The switch drain-source voltage v_{ds} and gate-source voltage v_{gs} at 100% load and 40% load for this method are given in Fig.13.

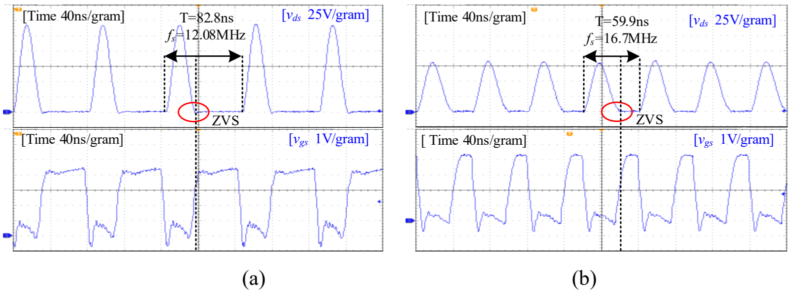

Fig. 13: Waveforms of v_{gs}, v_{ds} at 100% load and 40% load under the control method in this paper:(a) 100% load; (b) 40% load

Through the BDPFM control method proposed in this paper, the ZVS realization of the power tubes can be ensured under different loads and different switching frequencies.

To further illustrate the effectiveness of the control method in this paper, the losses of each component in the converter under different control methods and different loads are given below. As Fig.14.

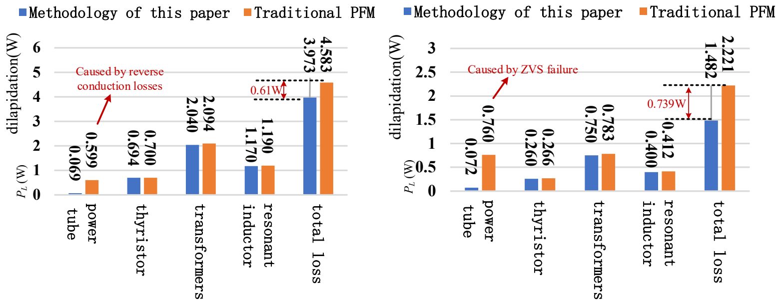

(a) (b)

Fig. 14: Loss disassembly of the converter at different loads and control methods: (a) 100% load; (b) 40% load

At 100% load, the GaN HEMT device under the traditional PFM control generates large reverse conduction loss, and the total loss of the power tube is 0.599 W. In contrast, under the BDPFM control proposed in this paper, the loss of the power tube is only 0.069 W. The control method in this paper reduces the loss of the power tube by 0.53 W, and reduces the total loss of the converter by 0.61 W (a reduction of 13.3%). At 40% load, the soft-switching failure of the GaN HEMT device under traditional PFM control produces large hard-switching losses, and the total power tube loss is 0.76 W. In contrast, the BDPFM control method proposed in this paper can reduce the power tube loss by 0.688 W and the total converter loss by 0.739 W (33.3% reduction).

4.2. Transient Experiment

To test the dynamic performance of the converter under BDPFM control and the mode switching function at light loads, load hopping experiments were carried out on the constructed model. It is shown in Fig.15.

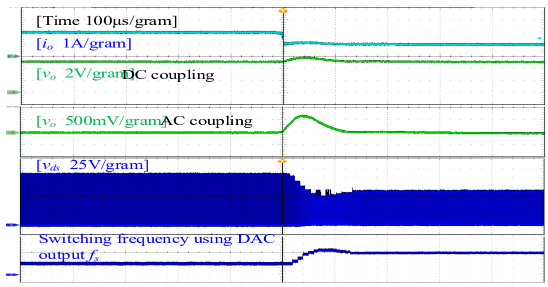

Fig. 15: Waveforms of $\boldsymbol{v_o}$, $\boldsymbol{i_o}$, and $\boldsymbol{v_{ds}}$ measured when switching from 100% load to 50% load and switching frequency using DAC outputs

The above figure gives the dynamic response waveforms of the output voltage v_O output current i_O, and switching node voltage v_{ds} when the converter is switched from 100% load to 50% load. To intuitively respond to the change of the converter's actual operating frequency during the dynamic response, the converter's switching frequency of 10 to 18 MHz is mapped into a voltage signal of 0 to 3.3 V. The converter initially operates at a lower switching frequency (12.08 MHz), and when the load is switched from 100% to 50%, the FM controller then raises the operating frequency of the converter to reduce the output power. As the switching frequency increases the output power gradually decreases; about 100 us after the load jump, the output voltage of the converter re-stabilizes, and the operating frequency at stabilization is 16.2 MHz .

4.3. Comparative Validation of Overall Performance

Fig.16 gives a comparison of the efficiency η of the converter under BDPFM control, conventional PFM and ON/OFF control. When the output current is $i_O = 1.2\,A$, the efficiency is 75. 1% for both this paper's method and under conventional PFM control. This is since the critical duty cycle of the converter is 0.5 at this time, and both this paper's method and the traditional PFM control are able to realize the ZVS of the power tubes. when the output current is less than 1.2 A, the ZVS of the power tubes under the traditional PFM control is invalid, which leads to a sharp decrease in the efficiency; when the output current is greater than 1.2A, the traditional PFM control produces a large reverse conduction loss, which reduces the efficiency of the converter. In contrast, the control method in this paper can realize the ZVS of the power tube in the full load range and avoid its reverse conduction at the same time. In addition, the control method in this paper can use the dynamic switching frequency to reduce the circulating current loss of the converter, to achieve a slightly higher efficiency than the ON/OFF control.

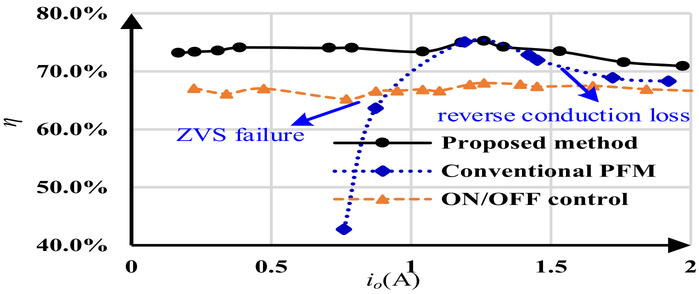

Fig. 16: Comparison of efficiency and output voltage ripple under different control methods: efficiency η;

A comparison of the output voltage ripple Δv_o of the converter under BDPFM control, conventional PFM and ON/OFF control is given in Fig.17. At full load, the output voltage ripple is 26 mV under the control method of this paper and 238 mV under ON/OFF control. Compared to ON/OFF control, the control method of this paper can reduce the output voltage ripple at full load by 89.1%.

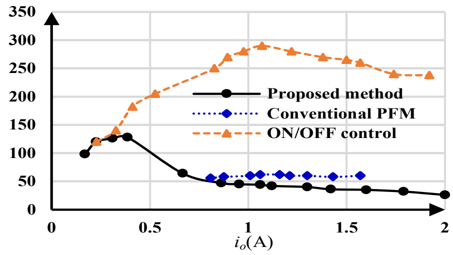

Fig. 17: Comparison of efficiency and output voltage ripple under different control methods: output voltage ripple Δv_o

Table I gives the performance comparison of different control methods. It can be seen that the control method in this paper has obvious advantages in terms of output voltage ripple. From another point of view, in applications with less stringent ripple requirements, the control method in this paper can effectively reduce the output filter capacitance and promote the miniaturization and integration of power supplies.

Table 1. Performance comparison of different control methods

Methods	*Vin*	*VOUT*	*η*	*ORV*	*Co*	*NORV*
paper	28 V	5 V	77%	26.3 mV	60.3 μF	7.8 V
VF ON/OFF	18 V	5 V	74%	153.6 mV	39.8 μF	60 V
MPL ON/OFF	18 V	5 V	75%	102.4 mV	100.2 μF	100V
Conventional ON/OFF	24 V	5 V	76%	176.7 mV	10.8 μF	29 V
	5 V	5 V/	79%	223.9 mV	20.5 μF	**330 V**

5. Acknowledgment

In this paper, a simplified circuit of UHF isolated resonant power converter is established based on the describing function and impedance fitting method, and the time-domain description of the converter at different switching frequencies is solved based on the model, and the critical duty cycle of ZVS at different switching frequencies is obtained based on the over-zero point of switching node voltage, and the BDPFM optimization and control strategy of UHF isolated resonant power converter is further proposed. control strategy for UHF isolated resonant power converter. The proposed strategy can ensure the realization of ZVS of power tubes and avoid reverse conduction loss under dynamic frequency, and at the same time greatly reduce the output voltage ripple of the converter. The controller can adjust the switching frequency to achieve output voltage regulation, and at the same time, calculate the critical duty cycle according to the real-time switching frequency, and turn on the switching node voltage immediately after it resonates to 0, to achieve ZVS and avoid reverse conduction of the power device. Through transient and transient comparison tests, the results show that the BDPFM control strategy proposed in this paper can reduce the output voltage ripple by 89.1% at 100% load, and the total loss of the converter can be reduced by 33.3% at 40% load.

6. References

[1] Kai Luo; Han Wang; Chao Gou, “A novel PWM/PFM control technique for transient improvement and high efficiency over a wide load range in buck DC-DC converter,” in press.

[2] Soheli Sairatun Nesa ; Sarowar, Golam ; Hoque, Md. Ashraful，“Design and analysis of a DC - DC buck boost converter to achieve high efficiency and low voltage gain by using buck boost topology into buck topology,” in press.

[3] Guan Yueshi; Shi Zhenyu; Wang Yijie, “An Isolated High Frequency DC-DC Converter Based on Class E Resonant Circuit,” in press.

[4] K. A Ghazi; L. Ben-Brahim, “Towards ultra-high frequency and high efficiency gate drive circuits,” in press.

[5] HARASHIMA Fumio, “A Study on Efficiency for Resonant Power Converter by Consideration of Circuits Design,” in press.

[6] Xing Tan; Xinbo Ruan; “Equivalence Relations of Resonant Tanks: A New Perspective for Selection and Design of Resonant Converters,”

[7] Honggang Sheng; Yunqing Pei; Fred Wang, “Impact of Resonant Tank Structures on Transformer Size for a High Power Density Isolated Resonant Converter,” in press.

[8] Yiming Chen; Jianping Xu; Jing Cao; “PWM-PFM hybrid controlled LCC resonant converter with wide ZVS range and narrow switching frequency variation,” in press.

[9] Changkyu Bai; Byeyongcheol Han; Kim Sooa; “A New Modulation Strategy to Operate Bidirectional Resonant Converter Under Extended Input Range,” in press.

[10] Hamed Tebianian, “Design and Implementation of High Frequency Resonant Power Converters,” in press.

[11] Hirakawa, Takashi; Hasegawa, Naoki; Nakamoto, Yuta; “Theoretical Analysis of Ideal Full-Bridge Rectifier with High-Frequency Input,” in press.

[12] Huafeng Xiao; Li Zhang; Zheng Wang; “A New Soft-Switching Configuration and Its Application in Transformerless Photovoltaic Grid-Connected Inverters,” in press.

[13] David Vegas; Maria Pampin; Perez-Cisneros, Jose-Ramon, “UHF Class-E Power Amplifier Design for Wide Range Variable Resistance Operation,” in press.

[14] David Vegas; Perez-Cisneros, Jose-Ramon; Ruiz, Nieves; “Load-Invariant Double Class-E/F2 Resonant Topology for UHF DC-DC Power Conversion,” in press.

[15] Qingyun Huang; Ruiyang Yu; Qingxuan Ma, “Predictive ZVS Control With Improved ZVS Time Margin and Limited Variable Frequency Range for a 99% Efficient, 130-W/in3 MHz GaN Totem-Pole PFC Rectifier,” in press.